Nonlinear Dynamics and Systems Theory, **21** (4) (2021) 420–433

Master-Slave Synchronization of a Planar 2-DOF Model of Robotic Leg

R. Ramírez-Ramírez [1], A. Arellano-Delgado [2], R. M. López-Gutiérrez [1], J. Pliego-Jiménez [3] and C. Cruz-Hernández [4*]

[1] *Engineering, Architecture and Design Faculty, UABC, Ensenada B.C., 22860, México.*
[2] *Engineering, Architecture and Design Faculty, CONACYT-UABC, Ensenada B.C., 22860, México.*
[3] *Department of Electronics and Telecommunications, CONACYT-CICESE, Ensenada B.C. 22860, México*
[4] *Department of Electronics and Telecommunications, CICESE, Ensenada B.C. 22860, México.*

Received: April 22, 2021; Revised: July 22, 2021

Abstract: In this paper, synchronization in the master-slave coupling scheme of two mechanical lower limbs, or legs, is numerically presented. In particular, we use the sliding mode control approach for trajectory tracking of the master's end-effector and, in addition, the slave's end-effector synchronizes with the master's end-effector. The synchronization studies reported in the literature have two main interesting results: phase synchronization and anti-phase synchronization. It is our perception that these two synchronization types appear in human movements such as jumping, sitting or standing (as phase movements), and walking, running or swimming (as anti-phase movements). This work pretends to replicate some of these movements in a prosthetic leg, where the prosthetic leg is the slave and the natural leg is the master. The contribution of this work is the use of the master-slave synchronization scheme, in conjunction with the sliding mode control method, conceived in the particular problem of people with an amputated leg. Simulation studies performed on two mechanical dynamical models of 2-DOF are presented to demonstrate the viability and performance of the proposed master-slave synchronization scheme.

Keywords: *synchronization; nonlinear control; position control; robotics; sliding mode control.*

Mathematics Subject Classification (2010): 70Q05, 94B50, 93D09.

* Corresponding author: mailto:ccruz@cicese.mx

1 Introduction

Many years and efforts have been required to develop humanoids. From the robot *Knight* to the robot *Advanced Step in Innovative Mobility (ASIMO)* or the robot *ATLAS* [1–3]. The *Knight* robot was developed by the Italian genius Leonardo Da Vinci in 1495, the ASIMO robot by Honda in 1986, and the ATLAS robot by Boston Dynamics in 2013. Both the ASIMO robot and the ATLAS robot involve, in addition to the mechanical engineering of the *Knight* robot, other disciplines such as electrical engineering, computation engineering, and control theory, among others. Despite the locomotive level reached by ASIMO and/or ATLAS, they still lack the grace, speed, and performance of the human being. As the locomotion of these humanoids resembles that of humans, we can use them as assistant robots [4] or assistants [5], for example, people with a leg amputation regain the ability to walk, swim, or jump [6–10]. On the other hand, the synchronization theory is of great interest in the scientific community due to the physical phenomena it can explain. For example, in nature, we can see the synchronization of the flash of fireflies, electronically reproduced in [11]. In communication systems, along with the theory of chaos, it is possible to encrypt any kind of information [12] that can be implemented with micro-controllers as in [13]. Synchronization patterns for inter-human coordination have been found in humanoid research [14]. For example, for sitting the limbs are in phase synchronized [15] and for walking they are in anti-phase synchronized [16]. Rodriguez-Angeles and Nijmeijer in [17] mention that, “The problem of robot synchronization can be seen as tracking paths between systems with an additional challenge that is not considered in tracking controllers of the trajectory”. In their publication, they synchronize two manipulator robots by using the state estimation for feedback, E. Cicek in [18] has used an adaptive controller, and Bondhus et. al. in [19] have used a PID controller. The main differences between this work and [17–19] are: 1) the control method used, 2) the synchronization time, and 3) the conception of the work in the particular problem in conjunction with the approach and potential application in the rehabilitation of people with an amputated leg. The contribution of this work is the synchronization of trajectories between two similar 2-degree of freedom (2-DOF) manipulator robot systems, under the master-slave coupling scheme, making use of the method of sliding mode control (SMC), conceived for the potential application for people with an amputated leg. In this case, the human’s limb (*thigh* and *shank*) is the master system and a 2-serial *link* mechanical system is the slave system.

In a potential experimental evaluation, the master lower extremity would send its position to the slave lower extremity (using sensors), which must follow the movements of the master system until the synchronization is achieved, either in phase or in anti-phase. For simulation reasons, the master system is also modeled as a 2-DOF serial link mechanical system. This work is organized as follows. In Section 2, the non-linear systems synchronization is explained. In Section 3, we describe the control scheme for tracking the paths of the master system and how the slave system couples with the master one to achieve synchronization. In Section 4, we present the dynamic model of a system with 2-DOF, which is used to model the thigh and shank. In Section 5, the control by the SMC method is presented, applied to both the master and the slave systems. Also, the stability proof based on Lyapunov’s theory is presented. In Section 6, the results obtained are shown in the simulation for a circular path, where the synchronization of the master-slave scheme is confirmed. Finally, in Section 7 some conclusions are reported.

2 Master-Slave Synchronization

Huygen's observations regarding the synchronization of two weakly coupled mechanical parameters reveal five types of synchronization [20]: 1) full or identical synchronization, 2) generalized synchronization, 3) phase synchronization, 4) anticipated or delay synchronization, and 5) envelope amplitude synchronization. The present work focuses on the phase synchronization for two mechanical systems with 2-DOF.

For two nonlinear dynamic systems synchronization, suppose a system described by

$$\dot{\boldsymbol{q}}_m = \boldsymbol{f}(\boldsymbol{q}_m), \tag{1}$$

where $\boldsymbol{f}$ is the non-linear vector at least twice differentiable and with a smooth curve. And $\boldsymbol{q}_m \in R^n$ is the *master system* state vector. The second, *slave system*, is defined by

$$\dot{\boldsymbol{q}}_s = \boldsymbol{h}(\boldsymbol{q}_s, \boldsymbol{u}), \tag{2}$$

where $\boldsymbol{u} \in R^n$ is the input signal to the system, $\boldsymbol{h}$ is the non-linear vector that, like $\boldsymbol{f}$, is at least twice differentiable. Let the synchronization error be given by

$$\boldsymbol{e}_s = \boldsymbol{q}_m - \boldsymbol{q}_s, \tag{3}$$

then the control objective is to design a signal $\boldsymbol{u} \in R^n$ in such a way that

$$\lim_{t\to\infty} \|\boldsymbol{e}_s(t)\| = 0, \tag{4}$$

where $\|\cdot\|$ is the Euclidean norm. This means that, when $t \to \infty$, the systems (1) and (2) are synchronized.

3 Synchronization Strategy

Two stages are needed to achieve synchronization for two 2-DOF mechanical systems under the master-slave scheme. In the first stage, the master system follows the position of the desired path, and in the second stage, the slave system follows the position of the master system, Figure 1 shows these two stages. The first stage is represented by white blocks, while the gray blocks represent the second stage.

In the first stage, the value of $\boldsymbol{\tau}_m$ is increased or decreased until $\boldsymbol{q}_d - \boldsymbol{q}_m = \boldsymbol{e}_m \approx 0$, which means that the desired trajectory is reached. In the second stage, the slave system takes $\boldsymbol{q}_m$ as the desired position and compares it with $\boldsymbol{q}_s$, when $\boldsymbol{q}_m - \boldsymbol{q}_s = \boldsymbol{e}_s \approx 0$, both systems are in phase synchronized. The master system follows the path indicated by the vector $\boldsymbol{x}_d = [x_d \quad y_d]^T$ with the Cartesian (x, y) values. The inverse *kinematics* convert them to angular values that are required by the master's system joints.

3.1 Direct and inverse kinematic

With the kinematics analysis, it is possible to calculate the end-effector's position, speed, and acceleration without considering the forces and torques causing the movement. The geometric relationship between the system link's joints and the reference frame is established. If the length and angles of the links are known, it is possible to compute the end-effector position in the Cartesian plane through the *direct kinematics.* On the other hand, if the lengths of the links and end-effector position in the Cartesian plane are

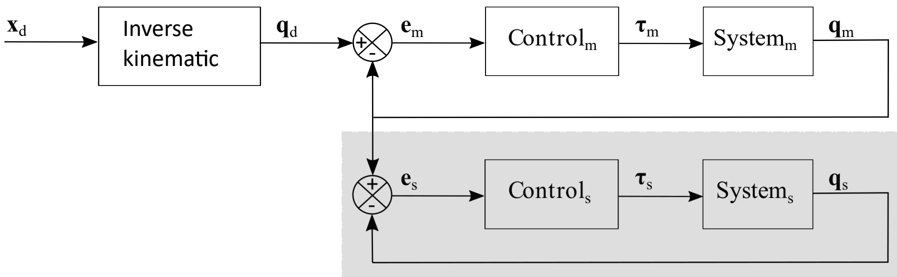

Figure 1: Master-slave synchronization scheme.

known, it is possible to compute the value of the link's angles through the *inverse kinematics*. For a two-link manipulator system in the Cartesian plane, as shown in Figure 2, the *direct kinematic* equations are:

$$x_m = l_{m1}\cos(q_{m1}) + l_{m2}\cos(q_{m1} + q_{m2}), \tag{5}$$

$$y_m = l_{m1}\sin(q_{m1}) + l_{m2}\sin(q_{m1} + q_{m2}), \tag{6}$$

where the master system link length variables are l_{m1} and l_{m2}, while the joint's angular variables are q_{m1} and q_{m2}.

On the other hand, the *inverse kinematics* equations to compute the joint's angular values are defined as follows:

$$q_{m2} = \tan^{-1}\left(\frac{\pm\sqrt{1-D^2}}{D}\right), \tag{7}$$

$$q_{m1} = \tan^{-1}(\frac{y_m}{x_m}) - \tan^{-1}\left(\frac{l_{m2}\sin(q_{m2})}{l_{m1} + l_{m2}\cos(q_{m2})}\right), \tag{8}$$

where

$$D = \frac{x_m^2 + y_m^2 - l_{m1}^2 - l_{m1}^2}{2l_{m1}l_{m2}}.$$

In this way it is possible to express the desired position $\boldsymbol{x}_d$ using either (5)-(6) or (7)-(8).

4 Dynamical Model of the 2-DOF Mechanism

The mechanism being used consists of two links connected in series with a revolute-type joint, therefore, it is a two-degree-of-freedom (2-DOF) mechanism. The synchronization strategy, described in Section 3, was simulated with an actuated 2-DOF mechanism that can perform any smooth trajectories in the Cartesian plane $(x,\ y)$. One 2-DOF mechanism for the master and another 2-DOF one for the slave. The dynamic model which represents N mechanical systems with 2-DOF is given by

$$H_i(\boldsymbol{q}_i)\ddot{\boldsymbol{q}}_i + C_i(\boldsymbol{q}_i, \dot{\boldsymbol{q}}_i)\dot{\boldsymbol{q}}_i + \boldsymbol{g}_i(\boldsymbol{q}_i) = \boldsymbol{\tau}_i, \quad i = m, s\,, \tag{9}$$

where the sub-index m is for the master system and the sub-index s is for the slave system, therefore, $\boldsymbol{q}_i = [q_{i1}\ q_{i2}]^T$, $\boldsymbol{\tau}_i = [\tau_{i1}\ \tau_{i2}]^T$ and

$$H_i = \begin{bmatrix} H_{11} & H_{12} \\ H_{21} & H_{22} \end{bmatrix}, C_i = \begin{bmatrix} C_{11} & C_{12} \\ C_{21} & C_{22} \end{bmatrix}, \boldsymbol{g}_i = \begin{bmatrix} g_{11} \\ g_{21} \end{bmatrix}, \tag{10}$$

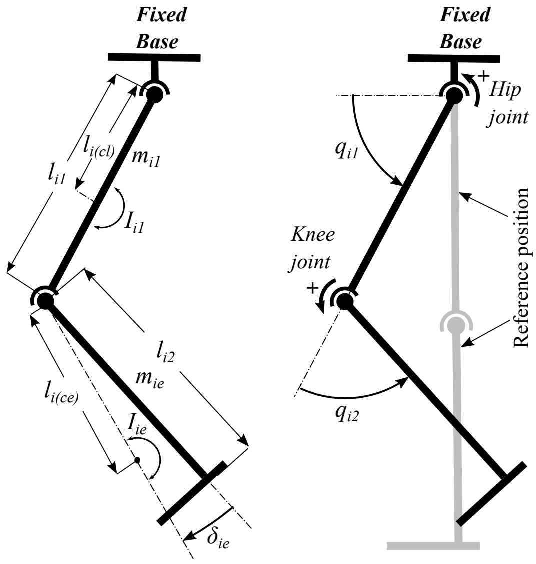

Figure 2: Master's mechanical system: thigh ($\boldsymbol{l_{i1}}$) and shank ($\boldsymbol{l_{i2}}$). The sub-index $\boldsymbol{i}$ is for either the master or the slave system.

where H_i is the inertia matrix, C_i is the Coriolis matrix, and $\boldsymbol{g}_i$ is the gravitational vector. Both τ_{i1} and τ_{i2} are the torques and moments of the joint's manipulator robot, i.e., the thigh and shank. Lastly, q_{i1} and q_{i2} are the angular positions of the thigh and shank as shown in Figure 2.

The elements of the matrices indicated in (9) are

$$
\begin{aligned}
&H_{11} = \alpha_i + 2\varepsilon_i \cos(q_{i2}) + 2\eta_i \sin(q_{i2}),\\
&H_{12} = \beta_i + \varepsilon_i \cos(q_{i2}) + \eta_i \sin(q_{i2}),\\
&H_{21} = \beta_i + \varepsilon_i \cos(q_{i2}) + \eta_i \sin(q_{i2})\\
&H_{22} = \beta_i,\\
&C_{11} = -2\varepsilon_i \sin(q_{i2} + 2\eta_i \cos(q_{i2}))\dot{q_{i2}},\\
&C_{12} = -\varepsilon_i \sin(q_{i2} + \eta_i \cos(q_{i2}))\dot{q_{i2}},\\
&C_{21} = \varepsilon_i \sin(q_{i2} + \eta_i \cos(q_{i2}))\dot{q_{i1}},\\
&C_{22} = 0,\\
&g_{11} = \varepsilon_i \rho_{i2} \cos(q_{i1} + q_{i2}) + \eta_i \rho_{i2} \sin(q_{i1} + q_{i2}) + (\alpha_i - \beta_i + \rho_{i1})\rho_{i2} \cos(q_{i1}),\\
&g_{12} = \varepsilon_i \rho_{i2} \cos(q_{i1} + q_{i2}) + \eta_i \rho_{i2} \sin(q_{i1} + q_{i2}).
\end{aligned}
$$

The variables α_i, β_i, ε_i, and η_i are related to the physical link's parameters [21], and are defined as follows:

$$\begin{aligned}
\alpha_i &= I_{i1} + m_{i1} l_{i(cl)}^2 + I_{ie} + m_{ie} l_{i(ce)}^2 + m_{ie} l_{i1}^2, \\
\beta_i &= I_{ie} + m_{ie} l_{i(ce)}^2, \\
\varepsilon_i &= m_{ie} l_{i1} l_{i(ce)} \cos(\delta_{ie}), \\
\eta_i &= m_{ie} l_{i1} l_{i(ce)} \sin(\delta_{ie}), \\
\rho_{i1} &= l_{i1} l_{i(cl)} - I_{i1} - m_{i1} l_{i1}^2, \\
\rho_{i2} &= g/l_{i1},
\end{aligned}$$

where

$$\begin{aligned}
m_{i1} &- thigh\, mass, \\
l_{i1} &- thigh\, length, \\
l_{i2} &- shank\, length, \\
l_{i(cl)} &- thigh\, center\, mass\, point, \\
I_{i1} &- thigh\, inertia, \\
m_{ie} &- shank\, mass, \\
l_{ie} &- shank\, length, \\
l_{i(ce)} &- shank\, center\, mass\, point, \\
I_{ie} &- shank\, inertia, \\
\delta_{ie} &- angle\, between\, the\, shank\, and\, shank\, center\, mass\, point.
\end{aligned}$$

It is important to say that the shank center mass point changes with a passive foot attached.

5 Controller Design

The control objective for many robot systems is to reach either a position, speed, or acceleration, and keep it within a specified range. A manipulator robot described in (9) is highly nonlinear, susceptible to the external disturbance or changes, and it is time variable. That is, the model's parameter values can vary for different positions, altitudes, loads, and model uncertainties [22–24]. The classical control theory for systems with these characteristics has low performance, and the asymptotic stability on follow-up tasks is not guaranteed. These issues are avoided with robust control approaches [25]. The sliding mode control (SMC) is a robust control that ensures the control objective even with the system's uncertainties [26]. Another characteristic of this control approach is that it can reduce the representation of a non-linear system by one order, which makes it easier to control compared to the classic control like PID control, see [27]. Some improvements of this control approach, mainly in mechanical systems, are presented in [28], which we use in this work.

5.1 Sliding mode control based on input-output stability

For a system like the one shown in (9), and assuming that α_i, β_i, ε_i, and η_i are known values, the master's and slave's position errors for the desired position path $\boldsymbol{q}_d$ are

$$\boldsymbol{e}_m = \boldsymbol{q}_d - \boldsymbol{q}_m, \quad \boldsymbol{e}_s = \boldsymbol{q}_m - \boldsymbol{q}_s. \tag{11}$$

Define

$$\dot{\boldsymbol{q}}_{mr} = \dot{\boldsymbol{q}}_d + \Lambda(\boldsymbol{q}_d - \boldsymbol{q}_m), \ \dot{\boldsymbol{q}}_{sr} = \dot{\boldsymbol{q}}_m + \Lambda(\boldsymbol{q}_m - \boldsymbol{q}_s), \tag{12}$$

where Λ is a positive diagonal matrix.

Since the dynamics of the robot is linear with respect to its parameters [28], we have

$$H_i(\boldsymbol{q}_i)\ddot{\boldsymbol{q}}_{ir} + C_i(\boldsymbol{q}_i, \dot{\boldsymbol{q}}_i)\dot{\boldsymbol{q}}_{ir} + \boldsymbol{g}_i(\boldsymbol{q}_i) = Y_i(\boldsymbol{q}_i, \dot{\boldsymbol{q}}_i, \dot{\boldsymbol{q}}_{ir}, \ddot{\boldsymbol{q}}_{ir})\boldsymbol{p}_i, \tag{13}$$

where

$$\boldsymbol{p}_i = [\alpha_i \quad \beta_i \quad \varepsilon_i \quad \eta_i]^T, \tag{14}$$

$$Y_i(\boldsymbol{q}_i, \dot{\boldsymbol{q}}_i, \dot{\boldsymbol{q}}_{ir}, \ddot{\boldsymbol{q}}_{ir}) = \begin{bmatrix} Y_{i1} & Y_{i2} & Y_{i3} & Y_{i4} \\ Y_{i5} & Y_{i6} & Y_{i7} & Y_{i8} \end{bmatrix} \tag{15}$$

with

$$\begin{aligned}
&Y_{i1} = \ddot{q}_{ir1} + \rho_{i2}\cos(q_{i1}),\\
&Y_{i2} = \ddot{q}_{ir2} - \rho_{i2}\cos(q_{i1}),\\
&Y_{i3} = 2\cos(q_{i2})\ddot{q}_{ir1} + \cos(q_{i2})\ddot{q}_{ir2} - 2\sin(q_{i2})\dot{q}_{i2}\dot{q}_{ir1} - \sin(q_{i2})\dot{q}_{i2}\dot{q}_{ir2} + \rho_{i2}\cos(q_{i1} + q_{i2}),\\
&Y_{i4} = 2\sin(q_{i2})\ddot{q}_{ir1} + \sin(q_{i2})\ddot{q}_{ir2} + 2\cos(q_{i2})\dot{q}_{i2}\dot{q}_{ir1} + \cos(q_{i2})\dot{q}_{i2}\dot{q}_{ir2} + \rho_{i2}\sin(q_{i1} + q_{i2}),\\
&Y_{i5} = 0,\\
&Y_{i6} = \ddot{q}_{ir1} + \ddot{q}_{ir2},\\
&Y_{i7} = \cos(q_{i2})\ddot{q}_{ir1} + \sin(q_{i2})\dot{q}_{i1}\ddot{q}_{ir1} + \rho_{i2}\cos(q_{i1} + q_{i2}),\\
&Y_{i8} = \sin(q_{i2})\ddot{q}_{ir1} - \cos(q_{i2})\dot{q}_{i1}\dot{q}_{ir1} + \rho_{i2}\sin(q_{i1} + q_{i2}).
\end{aligned}$$

The matrix $Y_i(\boldsymbol{q}_i, \dot{\boldsymbol{q}}_i, \dot{\boldsymbol{q}}_{ir}, \ddot{\boldsymbol{q}}_{ir})$ is known as the *dynamic regressor matrix.*

Using (11) and (12), the *sliding* variable for the master and slave ($i = m, s$) is determined by

$$\boldsymbol{\sigma}_i = \dot{\boldsymbol{q}}_{ir} - \dot{\boldsymbol{q}}_i = \dot{\boldsymbol{e}}_i + \Lambda e_i \tag{16}$$

and the Lyapunov function is defined as

$$V_i(t) = \frac{1}{2}\boldsymbol{\sigma}_i^T H_i(\boldsymbol{q}_i)\boldsymbol{\sigma}_i. \tag{17}$$

Therefore,

$$\begin{aligned}
\dot{V}_i(t) &= \boldsymbol{\sigma}_i^T H_i(\boldsymbol{q}_i)\dot{\boldsymbol{\sigma}}_i + \frac{1}{2}\boldsymbol{\sigma}_i^T \dot{H}_i(\boldsymbol{q}_i)\boldsymbol{\sigma}_i,\\
&= \boldsymbol{\sigma}_i^T H_i(\boldsymbol{q}_i)\dot{\boldsymbol{\sigma}}_i + \boldsymbol{\sigma}_i^T C_i(\boldsymbol{q}_i, \dot{\boldsymbol{q}}_i)\boldsymbol{\sigma}_i,\\
&= \boldsymbol{\sigma}_i^T [H_i(\boldsymbol{q}_i)(\ddot{\boldsymbol{q}}_{ir} - \ddot{\boldsymbol{q}}_i) + C_i(\boldsymbol{q}_i, \dot{\boldsymbol{q}}_i)(\dot{\boldsymbol{q}}_{ir} - \dot{\boldsymbol{q}}_i)],\\
&= \boldsymbol{\sigma}_i^T [H_i(\boldsymbol{q}_i)\ddot{\boldsymbol{q}}_{ir} + C_i(\boldsymbol{q}_i, \dot{\boldsymbol{q}}_i)\dot{\boldsymbol{q}}_{ir} + \boldsymbol{g}_i(\boldsymbol{q}_i) - \boldsymbol{\tau}_i]
\end{aligned} \tag{18}$$

with the sliding surface dynamics given by

$$H_i(\boldsymbol{q}_i)\dot{\boldsymbol{\sigma}}_i + C_i(\boldsymbol{q}_i, \dot{\boldsymbol{q}}_i)\boldsymbol{\sigma}_i = Y_i(\boldsymbol{q}_i, \dot{\boldsymbol{q}}_i, \dot{\boldsymbol{q}}_{ir}, \ddot{\boldsymbol{q}}_{ir})\boldsymbol{p}_i - \boldsymbol{\tau}_i. \tag{19}$$

The sliding mode based on the bound of (18) can be written as

$$\begin{aligned}
\dot{V}_i(t) &= -\boldsymbol{\sigma}_i^T [\boldsymbol{\tau}_i - (H_i(\boldsymbol{q}_i)\ddot{\boldsymbol{q}}_{ir} + C_i(\boldsymbol{q}_i, \dot{\boldsymbol{q}}_i)\dot{\boldsymbol{q}}_{ir} + \boldsymbol{g}_i(\boldsymbol{q}_i))],\\
&= -\boldsymbol{\sigma}_i^T [\boldsymbol{\tau}_i - Y_i(\boldsymbol{q}_i, \dot{\boldsymbol{q}}_i, \dot{\boldsymbol{q}}_{ir}, \ddot{\boldsymbol{q}}_{ir})\boldsymbol{p}_i]
\end{aligned} \tag{20}$$

and the control input as

$$\boldsymbol{\tau}_i = \overline{\boldsymbol{k}}_i \ sgn(\boldsymbol{\sigma}_i) = \begin{bmatrix} \overline{k}_{i1} \ sgn(\sigma_{i1}) \\ \overline{k}_{i2} \ sgn(\sigma_{i1}) \end{bmatrix}, \ i = m, s \,. \tag{21}$$

Consider the following region:

$$\mathbb{D}_{\sigma i} = \{\boldsymbol{\sigma}_i \mid \|\boldsymbol{\sigma}_i\| \le \delta_{\sigma i}\} \,. \tag{22}$$

Next, it will be shown that if $\boldsymbol{\sigma}_i \in \mathbb{D}_{\sigma i}$, then the position and speed errors, as well as the system paths $\boldsymbol{q}_i$ and $\dot{\boldsymbol{q}}_i$, are also bounded. According to (16), we have

$$\boldsymbol{e}_i(t) = e^{-\Lambda_i t}\boldsymbol{e}_i(0) + \int_0^t e^{-\Lambda_i(t-\vartheta)}\boldsymbol{\sigma}_i(\vartheta)d\vartheta. \tag{23}$$

From the previous equation, a position error bound can be calculated as follows:

$$\|\boldsymbol{e}_i\| \le \|\boldsymbol{e}_i(0)\| e^{-\underline{\lambda}_i t} + \frac{\delta_{\sigma i}}{\underline{\lambda}_i}\left(1 - e^{-\underline{\lambda}_i t}\right) \le \ \|\boldsymbol{e}_i(0)\| + \frac{\delta_{\sigma i}}{\underline{\lambda}_i}, \tag{24}$$

where $\underline{\lambda}_i \triangleq \lambda_{\min}\{\Lambda_i\}$. From the previous result, the speed error bound is determined by

$$\|\dot{\boldsymbol{e}}_i\| \le \bar{\lambda}\|\boldsymbol{e}_i(0)\| + \delta_{\sigma i}\left(\frac{\bar{\lambda}_i + \underline{\lambda}_i}{\underline{\lambda}_i}\right), \tag{25}$$

where $\bar{\lambda}_i \triangleq \lambda_{\max}\{\Lambda_i\}$. Since the desired trajectory $\boldsymbol{q}_{\rm d}(t)$ and its derivatives are bounded functions, the system trajectories $\boldsymbol{q}_i$ and $\dot{\boldsymbol{q}}_i$ are also bounded if $\|\boldsymbol{\sigma}_i\| \le \delta_{\sigma i}$. From the previous analysis, it is possible to determine the following elements bound for the regressor:

$$Y_i(\boldsymbol{q}_i, \dot{\boldsymbol{q}}_i, \dot{\boldsymbol{q}}_{\rm ir}, \ddot{\boldsymbol{q}}_{\rm ir}) = \left[Y_{i(nj)}\right], \left|Y_{i(nj)}\right| \le \bar{Y}_{i(nj)}. \tag{26}$$

To prove that the state $\boldsymbol{\sigma}_i$ is bounded, consider (17) which satisfies

$$\lambda_{{\rm h}i}\|\boldsymbol{\sigma}_i\|^2 \le V_i \le \lambda_{{\rm H}i}\|\boldsymbol{\sigma}_i\|^2, \tag{27}$$

where $\lambda_{{\rm h}i} = \lambda_{\min}\|H_i(\boldsymbol{q}_i)\}$ and $\lambda_{{\rm H}i} = \lambda_{\max}\|H_i(\boldsymbol{q}_i)\}$. The derivative of V_i along the system trajectories is given by

$$\begin{aligned} \dot{V}_i &= -\boldsymbol{\sigma}_i^{\rm T}\bar{\boldsymbol{k}}_i{\rm sign}(\boldsymbol{\sigma}_i) + \boldsymbol{\sigma}_i^{\rm T} Y_i(\boldsymbol{q}_i, \dot{\boldsymbol{q}}_i, \dot{\boldsymbol{q}}_{\rm ir}, \ddot{\boldsymbol{q}}_{\rm ir})\boldsymbol{p}_i \\ &= -\sum_{n=1}^{2}\bar{k}_i|\sigma_i| + \sum_{n=1}^{2}\sum_{j=1}^{4}\sigma_i\left[Y_{i(nj)}\right]p_{ij}. \end{aligned}$$

Consider (26) and suppose that the elements of the matrix $\bar{\boldsymbol{k}}_i$ are proposed as

$$\bar{k}_{i(n)} = \sum_{j=1}^{4}\bar{Y}_{i(nj)}\bar{p}_{ij} + \xi, \quad \xi > 0, \quad n = 1, 2 \,, \tag{28}$$

where

$$\boldsymbol{p}_i = [p_{i1} \quad p_{i2} \quad p_{i3} \quad p_{i4}]^T, \ |p_{in}| \le \overline{p_{in}} \ , \ n = 1, 2, 3, 4 \,.$$

The derivative of V_i satisfies

$$\dot{V}_i \leq -\sum_{n=1}^{2} |\sigma_i| \left(\sum_{j=1}^{4} \bar{Y}_{i(nj)} \bar{p}_{ij} + \xi \right) + \sum_{n=1}^{2} \sum_{j=1}^{4} |\sigma_i| \bar{Y}_{i(nj)} p_{ij} \leq -\xi \sum_{n=1}^{2} |\sigma_i| < 0. \tag{29}$$

Since the derivative is negative, the closed-loop variables are bounded, and $\boldsymbol{\sigma}_i$ tends to zero. To show the convergence in finite time, the following inequality will be used $\sum_{n=1}^{2} |\sigma_i| \geq \|\boldsymbol{\sigma}_i\|$. With consideration to the previous inequality and (27), an upper bound for (29) is given by

$$\dot{V}_i \leq -\xi \|\boldsymbol{\sigma}_i\| \leq -\alpha \sqrt{V}_i \,, \tag{30}$$

where $\alpha = \xi / \sqrt{\lambda_{\mathrm{h}i}}$. Or

$$D^+ W_i \leq -\alpha \,, \tag{31}$$

where $W_i = 2\sqrt{V_i}$. From the comparison lemma, we have $W_i(\|\boldsymbol{\sigma}(t)\|) \leq W_i(\|\boldsymbol{\sigma}(0)\|) - \alpha t$. Therefore, $\|\boldsymbol{\sigma}_i\| = 0$ in finite time. So, from (23), for a time $t_{\mathrm{R}} \leq W_i(0)/\alpha$, we have

$$\boldsymbol{e}(t) = e^{-\Lambda t} \boldsymbol{e}(0).$$

From the above, the position and velocity errors (16) converge to zero exponentially. Therefore, based on Lyapunov's theory of stability, the master's trajectory tracking and master-slave synchronization are assured.

6 Simulation

The synchronization of the master and slave systems, (9), is validated by a cyclic trajectory (circumference). The master system tracks this trajectory and the slave system tracks the master's end-effector position; both systems start at different initial conditions. Figure 3 shows the master and slave systems, the circular trajectory, the link's idle position (gray lines), the trajectory initial position (dotted lines), and the link's final position (black lines). The master system is represented by the left side links and the slave system is represented by the right side links.

The tracking of the trajectory is done without vertical control of both systems and without considering contact forces with any surface. The Matlab function ODE45 (Dorman-Prince) was used for the simulations with a variable integration step and relative tolerance of 1e-3, with duration of 15 s.

The physical parameters, control values, and initial conditions are presented below.

6.1 Desired trajectory

A circular path was chosen because it is predominantly used in therapeutic exercise equipment. Apply (32) with its center at $x_c = 0.5$ m, $y_c = -1.0$ m, and radius $r = 0.4$ m:

$$\boldsymbol{x}_d = \begin{bmatrix} x_c \\ y_c \end{bmatrix} - r \begin{bmatrix} \cos(\frac{1}{5}\pi t) \\ \sin(\frac{1}{5}\pi t) \end{bmatrix}. \tag{32}$$

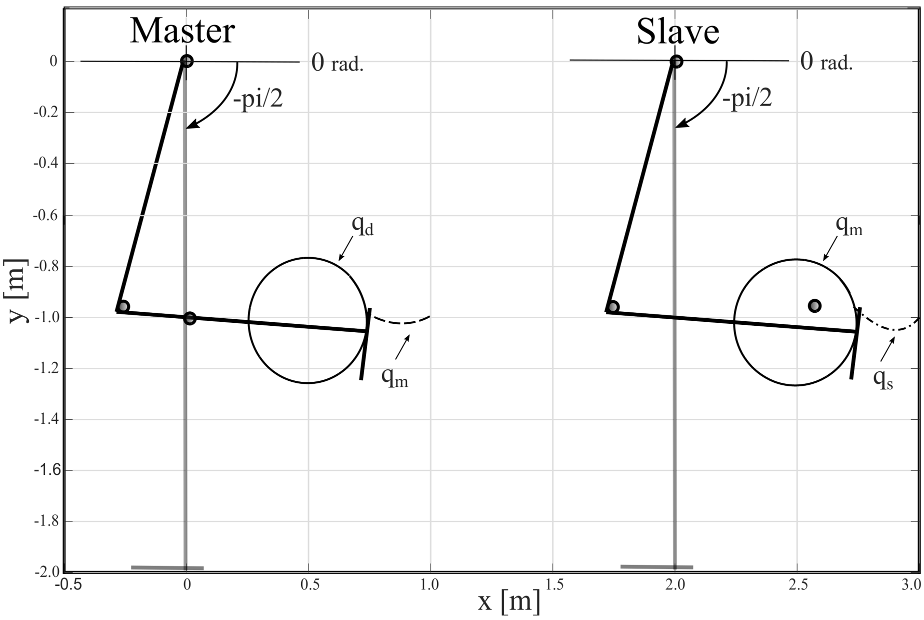

Figure 3: The tracking of the circular trajectory, master (left) and slave (right).

Variable	Value [unit]	Variable	Value [unit]
m_{m1}	1 [kg]	m_{s1}	1 1/5 [kg]
l_{m1}	1 [m]	l_{s1}	9/10 [m]
$l_{m(cl)}$	1/2 [m]	$l_{s(cl)}$	2/3 [m]
I_{m1}	1/12 [kg·m^2]	I_{s1}	0.081 [kg·m^2]
m_{me}	3 [kg]	m_{se}	3 1/4 [kg]
$l_{m(ce)}$	1 [m]	$l_{s(ce)}$	9/10 [m]
I_{me}	2/5 [kg·m^2]	I_{se}	13/30 [kg·m^2]
δ_{me}	0 [rads]	δ_{se}	0 [rads]
ρ_{m1}	$-7/12$	ρ_{s1}	-0.405
ρ_{m2}	9.81	ρ_{s2}	10.9

Table 1: Values of the parameters used.

6.2 Control parameter values

The values used in the simulation for the master and slave systems are shown in Table 1, from which the values for the vector $\boldsymbol{p_i}$ (14) are used in the computation of $\overline{\boldsymbol{k}}_{\boldsymbol{i}}$ in (28), which in turn, is required for the control input $\boldsymbol{\tau_i}$ in (21).

For sliding mode control simulations, the values of $\Lambda = [5 \quad 0; \quad 0 \quad 5]^T$ are chosen, which are applied in (12).

The master's initial conditions are $\boldsymbol{q_m} = [-\pi/2, \ \pi]$, and the slave's initial conditions are $\boldsymbol{q_s} = [-\pi/2+0.1, \ \pi]$, the values of the vector $\overline{\boldsymbol{p_i}}$ in (14) are $\overline{p}_m = |[6.7 \; 3.4 \; 3.0 \; 0.0]^T| + 0.50$ and $\overline{p}_s = |[6.2 \; 3.06 \; 2.6 \; 0.0]^T| + 0.50$, while $\xi = 0.1$. Finally, a saturation function is used instead of a switch function, with $\Delta = 0.05$.

6.3 Results

The master-slave synchronization established in (3) for two dynamic systems described by (9), with different initial positions and applying the control law (21) for a circular path (32), is described below. Applying the *inverse kinematic* by means of (7) and (8) we obtain q_{d1} and q_{d2}. The results in (21) are causing the angular position of the master's first link q_{m1} to move from -1,571 rads. to -1,671 rads., while the angular position of the slave's first link q_{s1} moves from -1,471 rads. to -1,671 rads. The angular position of the master's and slave's second link q_{m2}, q_{s2} moves from 1,571 rads. to 1,791 rads. The graphs in Figure 4 show these values and the time needed to reach the desired path.

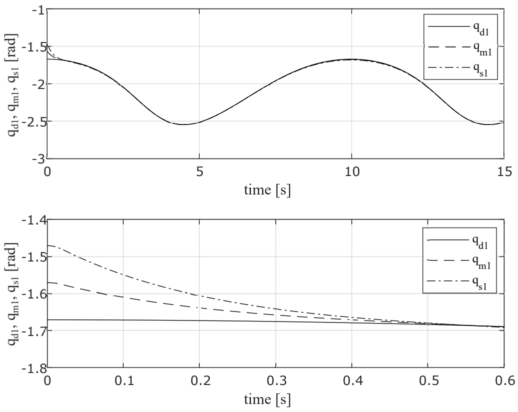

(a)

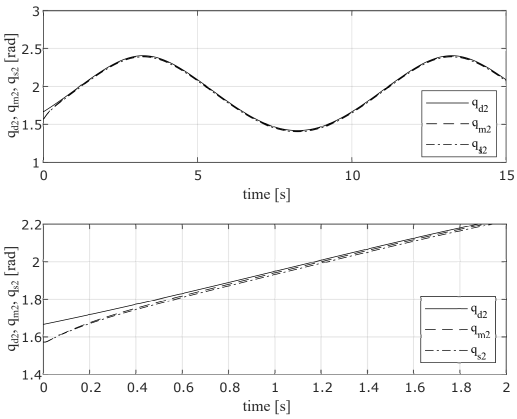

(b)

Figure 4: Link's positions during the desired trajectory tracking (32): a) Upper graphic $\boldsymbol{q_{d1}}$, $\boldsymbol{q_{m1}}$, and $\boldsymbol{q_{s1}}$ with $\boldsymbol{0 < t \leq 15}$, lower graphic with $\boldsymbol{0 < t \leq 0.6}$; b) Upper graphic $\boldsymbol{q_{d2}}$, $\boldsymbol{q_{m2}}$, and $\boldsymbol{q_{s2}}$ with $\boldsymbol{0 < t \leq 15}$, lower graphic with $\boldsymbol{0 < t \leq 2.0}$.

Finally, Figure 5a shows the control input $\boldsymbol{\tau}_i$ applied to q_{i1} and q_{i2} required to follow the desired path and synchronize the slave system with the master system, respectively.

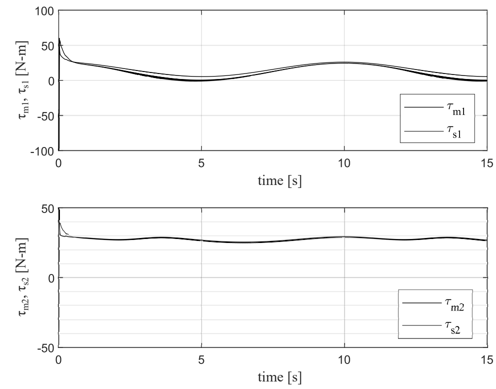

(a)

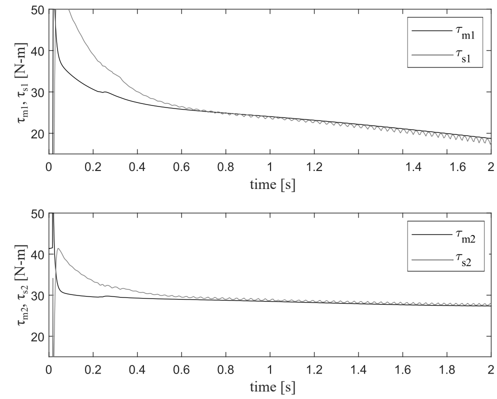

(b)

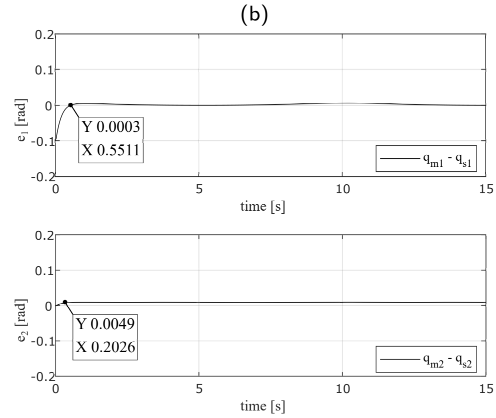

(c)

Figure 5: Input signal (21) during the desired trajectory tracking (32): a) Upper graphic $\boldsymbol{\tau_{m1}}$ and $\boldsymbol{\tau_{s1}}$, lower graphic $\boldsymbol{\tau_{m2}}$ y $\boldsymbol{\tau_{s2}}$, both with $\boldsymbol{0 < t \leq 15}$; b) Upper graphic $\boldsymbol{\tau_{m1}}$ and $\boldsymbol{\tau_{s1}}$, lower graphic $\boldsymbol{\tau_{m2}}$ y $\boldsymbol{\tau_{s2}}$, both with $\boldsymbol{0 < t \leq 2}$; c) Upper graphic $\boldsymbol{e_{s1}}$, lower graphic $\boldsymbol{e_{s2}}$.

Figure 5b shows a zoom out of these graphs to appreciate the switching effects *chattering* inherent in the control method by sliding modes, while the graph in Figure 5c shows that the synchronization error is below 1% of the amplitude of the signal $\boldsymbol{x}_d$ in $0.5\,s$ of the slave's first link and approximately $0.25\,s$ for the slave's second link. These results show that the synchronization is reached within the time reported in [17–19], which makes this synchronization scheme a suitable option.

7 Conclusions

Two systems synchronization by the master-slave scheme with the sliding mode control was simulated. It was possible to synchronize them, even with different initial positions, in $0.596\,s$. The graphs presented show that the master and slave tracking errors tend to zero. Therefore, it is feasible to synchronize a mechanical system that emulates a mechanical prosthetic leg with another similar system such as a human leg, where the human leg is the master system and the mechanical prosthetic leg, like a 2-DOF robotic system, is the slave system. The rehabilitation stage and exercises required for a person with a leg amputation are beyond the scope of this work. However, we believe that this proposed synchronization scheme is the basis for those who consider to implement it as part of the rehabilitation, where a circular path is used as a reference trajectory because the therapeutic exercise equipment has it as the main movement.

Acknowledgment

This work was supported by CONACYT through the Research Project on Basic Science, ref. 166654 (A1-S-31628).

References

[1] M. Rosheim. *Leonardo's Lost Robots*. Springer-Verlag, Berlin, Heidelberg, 2006.

[2] M. F. Silva, and J. A. T. Machado. A historical perspective of legged robots. *Journal of Vibration and Control* **13** (9–10) (2007) 1447–1486.

[3] E. Yoshida. Robots that look like humans: A brief look into humanoid robotics. *Mètode Science Studies Journal* **9** (2019) 143–151.

[4] T. Yan, M. Cempini, C. M. Oddo, and N. Vitiello. Review of assistive strategies in powered lower-limb orthoses and exoskeletons. *Robotics and Autonomous Systems* **64** (2015) 120–136.

[5] M. Dengd, Z. Ma, Y. Wang, H. Wang, Y. Zhao, Q. Wei, W. Yang, and C. Yang. Fall preventive gait trajectory planning of a lower limb rehabilitation exoskeleton based on capture point theory *Frontiers of Inf Technol Electronic Eng.* **20** (10) (2019) 1322–1330.

[6] A. M. Simon, N. P. Fey, K. A. Ingraham, A. J. Young, and L. J. Hargrove. Powered prosthesis control during walking, sitting, standing, and non-weight bearing activities using neural and mechanical inputs. In: *2013 6th International IEEE/EMBS Conference on Neural Engineering (NER)*, 2013, 1174–1177.

[7] R. D. Gregg, T. Lenzi, L. J. Hargrove, and J. W. Sensinger. Virtual Constraint Control of a Powered Prosthetic Leg: From Simulation to Experiments With Transfemoral Amputees. *IEEE Transactions on Robotics* **30** (6) (2014) 1455–1471.

[8] A. H. Shultz, B. E. Lawson, and M. Goldfarb. Running With a Powered Knee and Ankle Prosthesis. *IEEE Trans Neural Syst and Rehabil Eng.* **23** (3) (2015) 403–412.

[9] M. R. Tucker, O. Jeremy, A. Pagel, H. Bleuler, M. Bouri, O. Lambercy, J. R. Millan, R. Riener, H. Vallery and R. Gassert. Control Strategies for Active Lower Extremity Prosthetics and Orthotics: a Review. *Journal of NeuroEngineering and Rehabilitation* **12** (1) (2015).

[10] X. Zhang, W. Ge, H. Fu, R. Chen, T. Luo, and M. Hashimoto. A Human-Robot Interaction Based Coordination Control Method for Assistive Walking Devices and an Assessment of Its Stability. *Mathematical Problems in Engineering* **2018** (2018) 17 pages.

[11] A. Arellano-Delgado, C. Cruz-Hernández, R. M. López-Gutiérrez, and C. Posadas-Castillo. Outer Synchronization of Simple Firefly Discrete Models in Coupled Networks. *Mathematical Problems in Engineering* **2015** (2015) 14 pages.

[12] Y. Bolotin, T. Anatoli, and V. Yanovsky. Synchronization of Chaotic Systems. In: *Chaos: Concepts, Control and Constructive Use*. Springer-Verlag, Berlin, Heidelberg, 2009.

[13] M. A. Murillo-Escobar, C. Cruz-Hernández, F. Abundiz-Pérez, and R. M. López-Gutiérrez. Implementation of an improved chaotic encryption algorithm for real-time embedded systems by using a 32-bit microcontroller. *Microprocessors and Microsystems* **45** (Part B) (2016) 297–309.

[14] A. Mörtl, T. Lorenz, B. N. S. Vlaskamp et. al. Modeling inter-human movement coordination: Synchronization governs joint task dynamics. *Biological Cybernetics* **106** (4) (2012) 241–259.

[15] G. A. Leonov. Phase synchronization: Theory and applications. *Automation and Remote Control* **67** (10) (2006) 1573–1609.

[16] W. Liu, J. Xiao, X. Qian, and J. Yan. Antiphase synchronization in coupled chaotic oscillators. *Physical Review E* **73** (5) (2006) 4 pages.

[17] A. Rodriguez-Angeles, and H. Nijmeijer. Synchronizing Tracking Control for Flexible Joint Robots via Estimated State Feedback. *Journal of Dynamic Systems, Measurement, and Control* **126** (1) (2004) 162–172.

[18] A. Cicek, H. Dasdemir, and E. Zergeroglu. Coordinated synchronization of multiple robot manipulators with dynamical uncertainty. *Transactions of the Institute of Measurement and Control* **37** (5) (2015) 672–683.

[19] A. K. Bondhus, K. Y. Pettersen, and H. Nijmeijer. Master-Slave synchronization of robot manipulators: Experimental results. In: *IFAC Proceedings* **38** (1) (2005) 367–372.

[20] A. C. J. Luo. *Dynamical System Synchronization*. Springer-Verlag, New York, 2013.

[21] J. - J. E. Slotine, and W. Li. On the Adaptive Control of Robot Manipulators. *The International Journal of Robotics Research* **6** (3) (1987) 49–59.

[22] Y. Zhao. Study on predictive control for trajectory tracking of robotic manipulator. *Journal of Engineering Science and Technology Review.* **7** (1) (2014) 45–51.

[23] P. Skruch. A Terminal Sliding Mode Control of Disturbed Nonlinear Second-Order Dynamical Systems. *Journal of Computational and Nonlinear Dynamics* **11** (5) (2016).

[24] A. J. Muñoz-Vázquez, and F. Martínez-Reyes. Output Feedback Fractional Integral Sliding Mode Control of Robotic Manipulators. *Journal of Computational and Nonlinear Dynamics* **14** (5) (2019).

[25] V. Parra-Vega, S. Arimoto, Yun-Hui Liu, G. Hirzinger, and P. Akella. Dynamic sliding PID control for tracking of robot manipulators: theory and experiments. *IEEE Transactions on Robotics and Automation* **19** (6) (2003) 967–976.

[26] J. -J. E.Slotine, and W. Li. *Applied Nonlinear Control.* Prentice-Hall, Berlin, New Jersey, 1991

[27] A. Spiers, S. G. Khanaid, and G. Herrmann. *Biologically Inspired Control of Humanoid Robot Arms, Robust and Adaptive Approaches.* Springer International Publishing AG, Switzerland, 2016.

[28] J. Liu, and X. Wang. *Advanced Sliding Mode Control for Mechanical Systems.* Springer-Verlag, Berlin, Heidelberg, 2011.